

The Asiago-ESO/RASS QSO Survey. I.

The Catalog and the Local QSO Luminosity Function *

A. Grazian

Astronomy Department, University of Padua, I-35122 Padua, Italy

S. Cristiani ¹

European Southern Observatory, ST European Coordinating Facility, D-85748 Garching
bei München, Germany

V. D'Odorico

SISSA, I-34013 Trieste, Italy

A. Omizzolo

Vatican Observatory

and

A. Pizzella

European Southern Observatory, Casilla 19001, Santiago 19, Chile and Astronomy
Department, University of Padua, I-35122 Padua, Italy

*Based on material collected with the ESO-La Silla, Asiago, NOAO and VATT
telescopes

Received _____; accepted _____

submitted to the Astronomical Journal December 3, 2018

¹On leave from the Astronomy Department, University of Padua.

ABSTRACT

This paper presents the first results of a survey for bright quasars ($V < 14.5$ and $R < 15.4$) covering the North Hemisphere at galactic latitudes $|b| > 30$. The photometric database is derived from the GSC and USNO catalogs. Quasars are identified on the basis of their X-ray emission measured in the ROSAT All Sky Survey. The surface density of quasars brighter than 15.5 mag turns out to be $10 \pm 2 \cdot 10^{-3} \text{deg}^{-2}$, about 3 times higher than that estimated by the PG survey. The quasar optical Luminosity Function (LF) at $0.04 < z \leq 0.3$ is computed and shown to be consistent with a Luminosity Dependent Luminosity Evolution of the type derived by La Franca and Cristiani (1997) in the range $0.3 < z \leq 2.2$. The predictions of semi-analytical models of hierarchical structure formation agree remarkably well with the present observations.

Subject headings: clusters: quasars, general

1. Introduction

Quasar surveys provide basic information for the understanding of a number of astrophysical, cosmological and cosmogonical issues: the formation and evolution of galactic structures, the physics of the AGN phenomenon, the UV and X-ray backgrounds.

The general behaviour of the QSO optical luminosity function (OLF) is well established in the redshift interval $0.3 < z < 2.2$ for which color techniques provide reliable selection criteria (see Hartwick and Schade 1990, Boyle 1992, Hewett and Foltz 1994, for a review of the subject). A pure luminosity evolution (PLE) appears to reasonably describe the data in the interval $0.6 < z < 2.2$. In the range $0.3 < z < 0.6$ the OLF appears to be flatter than observed at higher redshifts (Goldschmidt et al. 1992), requiring a luminosity dependent luminosity evolution (LDLE, La Franca and Cristiani, 1997 LC97). This departure from a PLE provides an interesting clue for the physical interpretation of the QSO evolving population (Cavaliere et al. 1997, LC97). The present observational evidence, however, relies on a relatively small number of objects: in the $0.3 < z < 0.6$ range for $M_B < -25$, 32 QSOs are observed by LC97 instead of the 19 expected from the best-fit PLE model. Analogous results by Köhler et al. (1997) and Goldschmidt and Miller (1998) are likewise based on very small samples.

To provide a statistically solid basis for the LDLE pattern and to investigate whether such a trend persists (and possibly becomes more evident) at redshifts lower than 0.3, we decided to carry out a new large-area survey of quasars at bright optical fluxes. A typical apparent magnitude for a $M_B = -24$ QSO at $z \sim 0.1$ is in fact $B \sim 14.5$ and the surface density of these objects, according to previous surveys (e.g. the BQS, Schmidt & Green 1983), is expected to be less than 10^{-3} per sq.deg., requiring an efficient selection criterion and the coverage of a significant fraction of the whole sky in order to collect a meaningful sample.

In Sect.2 we describe the photometric database from which optical fluxes have been derived, in Sect.3 the criteria followed to select the candidates, in Sect.4 the spectroscopic follow-up, in Sect.5 the derived quasar counts and the optical luminosity function and in Sect.6 a few consequences for model scenarios.

2. The Photometric Database

A number of photometric catalogues are available in the literature, covering a substantial fraction of the celestial sphere down to the optical magnitudes of interest for the present survey. We have chosen the *USNO* (Monet et al. 1996), *GSC* (Lasker et al. 1988) and the *DSS* (Digitized Sky Survey).

To test the accuracy of the photometric calibration of these catalogues, we have used as a comparison in the Northern sky the photometric standards of Landolt (1992). In the Southern hemisphere we have used 446 standards derived from the input catalog used to calibrate the photometric material of the Homogeneous Bright Quasar Survey (HBQS, Cristiani et al. 1995). From both samples only relatively bright ($12.5 \leq V \leq 16.0$) and not too red ($B - R \leq +1.0$) stars have been chosen in order to match the characteristics of the quasars searched for in this survey.

We finally defined three flux-limited samples adopting as photometric reference:

1. in the Northern hemisphere objects with $11.0 < V_{GSC} \leq 14.5$ in the GSC catalog. The relation between the V_{GSC} band and the corresponding Johnson V turned out to be:

$$V_{GSC} = V - 0.21 \quad (1)$$

with $\sigma_V = 0.27$ mag. 7 (4%) of the 183 Landolt stars used for this comparison were not found in the GSC catalog.

2. in the Northern hemisphere objects from the USNO catalog with $13.5 < R_{USNO} \leq 15.4$.

The relation between the R_{USNO} band and the corresponding Johnson-Kron-Cousins R turned out to be:

$$R_{USNO} = R_{JKC} + 0.096 \quad (2)$$

with $\sigma_{R_{USNO}} = 0.267$ mag. No correlation between the residuals of $R_{USNO} - R_{JKC}$ and the color $(B - R)_{JKC}$ has been found. According to Monet et al. (1996), the internal magnitude estimators for stars in the USNO catalog are probably accurate to something like 0.15 magnitudes over the range $R_{USNO} = 12$ mag to $R_{USNO} = 19$ mag, but the systematic error arising from the plate-to-plate differences is at least 0.25 magnitudes in the Northern hemisphere, consistent with our estimates.

3. in the Southern hemisphere we have derived B_J magnitudes from the Digitized Sky Survey (DSS). Small scans (“postage stamps” of $2' \times 2'$) of each object of interest and of 20-50 surrounding objects with known GSC B_J magnitudes were extracted from the DSS. The magnitude of the object of interest was then calibrated against the GSC objects. In this way a σ_{B_J} of 0.10 mag was obtained in the interval $12.0 < B_J < 15.5$.

3. The Selection of the Sample

3.1. The ROSAT All Sky Survey

In order to pick out the bright quasars from the overwhelming number of stars in the same magnitude range, an efficient selection criterion is required. A convenient possibility is offered by the X-ray emission, which is a key signature of the AGN phenomenon.

The ROSAT All Sky Survey (hereafter RASS, Voges 1992) was carried out during the period July 1990/February 1991 with the PSPC and has produced a photometric database in the Soft-X (0.1-2.4 KeV). This shallow survey covers almost the entire sky at a

bright level (10^{-13} erg cm $^{-2}$ sec $^{-1}$) and initially contained 60000 sources. A more evolved reduction analysis, SASS-II, has produced the RASS Bright Source Catalogue (RASS-BSC, Voges et al. 1999), a sample of 18811 X-ray sources at a limiting flux level of 0.05 cps^2 all over the sky.

The main constituents of the RASS catalogue are AGNs and peculiar stars (CV, M stars, K stars, WDs, X-ray binaries and coronally active stars), but there are also cluster of galaxies, BL Lacs, SN remnants, neutron stars and normal galaxies (or starbursts). A convenient way to distinguish/isolate AGNs is the comparative analysis of their soft-X/optical properties (Hasinger et al. 1998).

We have cross-correlated the RASS catalogue with the photometric databases described in the previous section for sources at galactic latitudes $|b| \geq 30$ deg and with a RASS-BSC exposure time ≥ 300 s, i.e. $flux \geq 0.05$ cps . Sources classified as extended in the RASS have been disregarded, while no selection based on optical morphology was applied. We have looked for optical objects in the range $11.0 < V_{GSC} \leq 14.5$ and $13.5 < R_{USNO} \leq 15.4$ around the RASS sources, adopting a matching radius three times the RMS positional uncertainty of each entry in the RASS catalog (typically $3 \times 12''$). In this way very few (of the order of 0.1%) true identifications in the desired optical range are missed. Misidentifications, i.e. “X-ray quiet” AGN in the desired optical magnitude range falling by chance in the RASS error-box, are also possible, but extremely unlikely, given the low surface density of these bright AGN and are in any case irrelevant for the present work, which aims at the definition of the local *optical* QSO LF.

The resulting catalogue covers 8164 square degrees in the North and 5855 square

² cps is the ‘counts per second’ of a source and is a measure of the flux, when a precise X-soft spectrum is considered. For $F(\nu) \propto \nu^{-1}$ 0.05 cps correspond to 10^{-13} erg s $^{-1}$ cm $^{-2}$.

degrees in the South.

3.2. The α_{ox} distribution of quasars and the Selection Criteria

For each source the α_{ox} index was computed as $\alpha_{ox} = -0.408 \log cps - 0.163R + 3.65$ or $\alpha_{ox} = -0.428 \log cps - 0.171V + 3.84$ or $\alpha_{ox} = -0.483 \log cps - 0.193B_J + 4.20$.

To obtain an estimate of the intrinsic distribution of the α_{ox} of quasars we have plotted the observed B , V or R magnitudes vs. the $\log cps$ for the $0.04 < z \leq 0.3$ quasars listed in the 8th edition of the Véron catalog (VV98, 1998). Fig. 1 shows the result for northern QSOs and R magnitudes.

EDITOR: PLACE FIGURE 1 HERE.

In this diagram the locus $\alpha_{ox} = \text{const}$ is represented by a straight diagonal line. “X-ray quiet” objects, i.e. with a flux $\leq 0.05 \text{cps}$ to the left of the vertical continuous line, are missed in the RASS. If we assume that the intrinsic distribution of the α_{ox} is not a function of the apparent luminosity (Yuan, Siebert and Brinkmann, 1998), selecting objects with $\alpha_{ox} < \alpha_{max}$ (i.e. “X-ray loud”) and optically brighter than a convenient limit will provide a sample with a degree of incompleteness that is not a function of the apparent magnitude. For example, in the case of the USNO database the limit in R turns out to be $R < (3.65 - \alpha_{max} - 0.408 \log cps_{min})/0.163 = 25.64 - 6.13\alpha_{max}$. If we adopt (see Fig. 1) an $\alpha_{max} = 1.7$ at magnitudes brighter than $R = 15.4$ only the objects with $\alpha_{ox} > \alpha_{max}$ will be missed.

Tab. 1 lists the interval of optical magnitudes and the corresponding limit on α_{ox} chosen for the USNO, GSC and DSS sub-samples. The last column shows the degree of completeness estimated on the basis of the fraction of quasars of the VV98 found with the

adopted criterion.

EDITOR: PLACE TABLE 1 HERE.

Examining the properties of the VV98 quasars in terms of the various RASS parameters, we have found two further empirical criteria, based on the hardness ratios $HR1$ and $HR2$ (Voges et al. 1999), to increase the effectiveness of the selection without affecting its completeness:

1. $-0.9 \leq HR1 \leq 0.9$, where $HR1$, the hardness ratio 1 is defined as $(A - B)/(A + B)$, with the ROSAT-PSPC count rates A in the hard band ($0.5 \div 2.0$ keV) and B in the soft band ($0.1 \div 0.4$ keV).
2. $-0.6 \leq HR2 \leq +0.8$, where $HR2$, the hardness ratio 2, is defined as $(C - D)/(C + D)$, with the ROSAT-PSPC count rates C in the hard band ($0.9 \div 2.0$ keV) and D in the soft band ($0.5 \div 0.9$ keV).

4. Spectroscopic Follow-up

In the following we concentrate our discussion on the sample of Northern objects, for which the follow-up spectroscopy is more advanced. The Southern sample will be described elsewhere. The list of the quasar candidates and the results of the spectroscopy are reported in Tab. 2. It should be noted that Tab. 2 cannot be considered a list of optical identifications of X-ray sources. The cross-correlation procedure defined in the previous section aims at finding optical objects in a desired magnitude range around X-ray sources. In some cases an entry in Tab. 2 may exist even if the true identification of the X-ray source is another (typically fainter) optical object. For example, even if the optical counterpart of the RASS source J013624.3+205712 is known to be the QSO 3C47.0, with $V \simeq 18.1$ and

$z = 0.425$, in Tab. 2 we list an object of $R_{USNO} = 14.7$ which happens to fulfill the criteria of the cross-correlation.

EDITOR: PLACE TABLE 2 HERE.

The follow-up observations of the QSO candidates have been carried out at the 1.8m telescope in Asiago with a Boller and Chivens Spectrograph or with the Asiago Faint Object Spectrograph and Camera (AFOSC), at the 1.5m ESO, 1.5m Danish and NTT telescopes in La Silla with a Boller and Chivens Spectrograph, DFOSC and EMMI respectively and with the 90" telescope at Kitt Peak. The resolution of the spectra ranges between 10 and 30 Å.

The reduction process used the standard MIDAS facilities (Banse et al., 1983) available at the Padua Department of Astronomy and at ESO Garching. The raw data were sky-subtracted and corrected for pixel-to-pixel sensitivity variations by division with a suitably normalized exposure of the spectrum of an incandescent source (flat-field). Wavelength calibration was carried out by comparison with exposures of He-Ar, He, Ar and Ne lamps. Relative flux calibration was carried out by observations of spectrophotometric standard stars (Oke, 1990).

The identification classes are: *AGN* = emission-line object, irrespective of the line width; *STAR* = star; *GAL* = galaxy; *BL* = BL Lac object. Identifications as BL Lac or Galaxy have been taken from the NASA/IPAC Extragalactic Database (NED). Uncertain identifications and redshifts are indicated with a colon (:).

In order to test the reliability of our selection, additional candidates, selected with less restrictive criteria than those reported in the previous section, were observed. They are reported in Tab. 3. The spectra of the AGNs found during the follow-up spectroscopy are shown in Fig. 2.

EDITOR: PLACE TABLE 3 HERE.

EDITOR: PLACE FIGURE 2 HERE.

5. First Results

The spectroscopic observations of the Northern sample are still incomplete: only 45% of the candidates have been identified. Different areas of the sky, in particular different strips in right ascension, have been observed down to different magnitude limits. Tables 4-5 list the extension of the area covered with a complete spectroscopic follow up as a function of the limiting magnitude.

In the following computations we have adopted for the Northern sample the “effective areas” listed in Tabs. 4-5, which take into account the incompleteness factors estimated in the previous sections.

EDITOR: PLACE TABLE 4 HERE.

EDITOR: PLACE TABLE 5 HERE.

5.1. Quasar Counts

Fig. 3 shows the LogN-LogS relation of QSOs brighter than $M_B = -23$ mag³ with $z \geq 0.04$, for the USNO and GSC subsamples together. The LogN-LogS has been computed

³In the present paper the K-corrections are computed on the basis of the composite spectrum of Cristiani and Vio (1990), galactic extinction is taken into account according

with the $\sum 1/Area_{max}$ method, a convenient approach when the various sub-areas have very different magnitude limits.

EDITOR: PLACE FIGURE 3 HERE.

The LogN-LogS relation found in the present survey is consistent with a single power-law distribution with the slope 0.67 reported by Köhler et al. (1997) for QSOs with $0.07 \leq z \leq 2.2$, with a slightly higher normalization: if we fix $\beta = 0.67$ in a $\log N = \beta B + k$ relation, we find $k = -12.15^{+0.17}_{-0.19}$. If we restrict our sample to $z > 0.07$ we find $k = -12.2 \pm 0.2$, in agreement with the normalization, $k = -12.4$, of Köhler et al. (1997).

A comparison with the Palomar Bright Quasar Survey (BQS, Schmidt & Green 1983) shows that at $B \sim 15.5$ the cumulative BQS counts are about a factor 3 lower. This confirms previous findings by Goldschmidt et al.(1992), LC97, Köhler et al. (1997).

EDITOR: PLACE TABLE 6 HERE.

5.2. The QSO Luminosity Function at $0.04 < z \leq 0.3$

A preliminary, cursory analysis of the QSO optical LF has been carried out on the basis of the present sample. A more detailed discussion of the complete spectroscopic database will be developed elsewhere (Grazian and Cristiani, in preparation). To compute the LF at $0.04 < z \leq 0.3$ we have used the generalized $1/V_{max}$ “coherent” estimator (Avni & Bahcall, 1980) in a slightly modified version which tries to estimate in an unbiased

to Burstein and Heiles (1982). The values $q_0 = 0.5$, and $H_0 = 50$ Km/s/Mpc are adopted throughout.

manner the volume-luminosity space “available” to each object (cf. the method of Page & Carrera, 1999) and takes into account the evolution of the LF within the redshift interval. Errors were estimated from Poisson statistics (Gehrels, 1986). The data values of the LF at $0.04 < z \leq 0.3$ are given in Tab. 7.

EDITOR: PLACE TABLE 7 HERE.

Figures 4a and 4b show the comparison of the newly derived QSO LF at $0.04 < z \leq 0.3$ with data at higher redshift, up to $z = 2.2$ (LC97), and with a PLE and an LDLE parameterization, respectively. The points in the range $0.04 < z \leq 0.3$ are the result of the present survey, the data in the other redshift ranges are derived from LC97. No effort has been made in the derivation of the LF at $0.04 < z \leq 0.3$ to subtract off the luminosity of the host galaxy.

EDITOR: PLACE FIGURE 4 HERE.

The PLE parameterization is the global best fit to the QSO LF derived in the interval $0.3 < z < 2.2$ by LC97 (Model B), who found it to be inconsistent with the data at $0.3 < z < 0.6$ at a 3σ level. The present result confirms and strengthens the conclusion of LC97: if we compare the prediction of the Model B PLE of LC97 in the range $0.04 < z \leq 0.3$, a $\chi^2 \simeq 14$ for the 5 data points of Tab. 7 is derived, corresponding to a formal probability of 1.9%.

Fig. 4b shows that an LDLE parameterization of the type of Model C of LC97 can reproduce the data in a much more satisfactory way. The best agreement with the data from $z = 0.04$ to $z = 2$ is obtained, assuming the functional form (LC97)

$$\Phi(M_B, z) = \frac{\Phi^*}{10^{0.4[M_B - M_B^*(z)](\alpha+1)} + 10^{0.4[M_B - M_B^*(z)](\beta+1)}} \quad (3)$$

with

$$M_B^*(z) = M_B^*(z=2) - 2.5k \log[(1+z)/3] \quad (4)$$

and

$$\text{for } M_B \leq M_B^*(z) : k = k_1 + k_2[M_B - M_B^*(z)]e^{-z/.40} \quad (5)$$

$$\text{for } M_B > M_B^*(z) : k = k_1$$

where α and β correspond to the faint-end and bright-end slopes of the optical LF, respectively and $M_B^*(z=2)$ is the magnitude of the break in the double power-law shape of the LF at $z=2$. The actual values adopted in the LDLE parameterization are: $\Phi^* = 9.8 \times 10^{-7} \text{mag}^{-1} \text{Mpc}^{-3}$, $M_B^*(z=2) = -26.3$, $k_1 = 3.33$, $k_2 = 0.37$, $\alpha = -1.45$, $\beta = -3.76$, providing a χ^2 probability $\simeq 58\%$ in the range $0.04 < z \leq 0.3$ when compared to the 5 data points of Tab. 7.

6. Discussion

Franceschini et al. (1994) and La Franca et al. (1995) have shown that the QSO emission in the soft-X and at visible wavelengths scales linearly. A confirmation of the constant ratio L_X/L_O and independence both from L_O and from z comes from Yuan et al. (1998). Boyle et al. (1994) derived a XLF comparable to the QSO OLF known at that epoch with an evolutionary rate $L_X(z) = L_X(0)(1+z)^{3.25}$, similar to the optical one. These works favor a scenario in which essentially the same QSO population is observed, both in the soft-X and in the optical. In this way the flattening of the OLF observed in the present survey should be reflected in a flattening in the corresponding soft-X LF. Indeed Miyaji et al. (1999) show that the bright part of the 0.5-2 keV LF flattens with decreasing redshift from a value $1+\beta \simeq 3.5$ at $0.4 < z < 0.8$ to $1+\beta \simeq 2.6$ at $0.015 < z < 0.2$, which is similar to what we observe in the optical: $1+\beta \simeq 3.7$ at $0.6 < z < 1.0$ and $1+\beta \simeq 3.1$ at

$0.04 < z \leq 0.3$.

The decline of the space density of quasars from a peak around redshift 2 to the present epoch has been modeled by several authors in the framework of hierarchical theories of structure formation (Cattaneo 1999, Haiman and Menou 1999, Kauffmann and Haehnelt, Monaco et al. 1999). In particular Kauffmann and Haehnelt (1999, KH99) have attempted to reproduce quantitatively the evolution of the quasar number density incorporating a scheme for the growth of massive black holes (MBHs) into semi-analytical models following the evolution of galaxies in CDM-dominated scenarios. Together with the decrease in the merging rates and in the amount of gas available to fuel the MBHs, which are built-in features of the semi-analytic models, KH99 assume an increase of the timescale for gas accretion in order to reproduce the steep decline in the number density of quasars from $z \sim 2$ to $z = 0$. Other authors have followed similar recipes assuming a decreasing mass accretion (Haiman and Menou 1999), or a decreasing efficiency of the accretion (Cattaneo 1999), or a delayed quasar activity with respect to the dynamical formation of the halos with a longer delay for smaller halos (Monaco et al. 1999).

As can be seen from Fig. 17 of KH99, the semi-analytical models have difficulties in reproducing the steep decrease of the QSO density at low redshift that is commonly measured (Hartwick and Schade 1990). The most promising scenario is a Λ CDM, in which the accretion timescale, t_{acc} , is assumed to vary in the same way as the host galaxy dynamical time ($t_{\text{acc}} \propto [0.7 + 0.3(1+z)^3]^{-1/2}$). This model is able to reproduce the evolution of the galaxy LF and of the cold gas content of galaxies, but is apparently predicting a too slow quasar decline. The present data significantly reduce this disagreement in the sense that the higher quasar space density measured in our survey corresponds fairly well to the Λ CDM semi-analytical predictions, as shown in Fig. 5.

EDITOR: PLACE FIGURE 5 HERE.

It is a pleasure to thank A. Wicenec for his invaluable help with the photometric database and F.La Franca, M. Haehnelt and G.Kauffmann for enlightening discussions. We are indebted to Mira and Philippe Véron whose indications helped us to improve significantly the accuracy of the identifications. We would also like to thank an anonymous referee for several useful comments which improved the paper. AG acknowledges the generous hospitality of ESO during two visits to Garching. This work is based on photographic data obtained using The UK Schmidt Telescope. The UK Schmidt Telescope was operated by the Royal Observatory Edinburgh, with funding from the UK Science and Engineering Research Council, until 1988 June, and thereafter by the Anglo-Australian Observatory. Original plate material is copyright (c) of the Royal Observatory Edinburgh and the Anglo-Australian Observatory. The plates were processed into the present compressed digital form with their permission. The Digitized Sky Survey was produced at the Space Telescope Science Institute under US Government grant NAG W-2166. The NASA/IPAC Extragalactic Database (NED) is operated by the Jet Propulsion Laboratory, California Institute of Technology, under contract with the National Aeronautics and Space Administration.

Table 1. Selection Criteria and Completeness

Sub-sample	Magnitude Interval	α_{ox}	Completeness max	Completeness N_{found}/N_{VV98}	%
USNO	$13.5 < R < 15.4$	1.7	24/36		68
GSC	$12.5 < V < 14.5$	1.9	5/8		63
DSS	$12.6 < B_J < 15.2$	1.9	8/9		89

Table 2. THE USNO SAMPLE

Name (1RXS)	R.A.	Declination	R_{USNO}	V_{GSC}	z	Type
J000150.9+111705	00 01 50.6	+11 16 47.6	15.10		0.158	AGN
J001031.3+105832	00 10 31.0	+10 58 29.6	13.60	14.66	0.089	AGN
J002337.1+044220	00 23 37.2	+4 42 22.3	14.30	15.13	0.081	AGN
J002811.6+310342	00 28 10.8	+31 03 47.8	15.30		0.500	AGN
J002913.9+131605	00 29 13.7	+13 16 03.6	15.30	15.23	0.142	AGN
J004240.8+301742	00 42 41.6	+30 17 43.9	14.40			
J005154.8+172552	00 51 54.8	+17 25 58.4	15.30		0.064	AGN
J013556.7+231605	01 35 58.5	+23 15 56.5	15.20			
J013624.3+205712	01 36 25.3	+20 56 49.6	14.70			
J014239.9+000514	01 42 38.4	+0 05 14.9	15.30			
J015242.1+010040	01 52 41.9	+1 00 25.1	14.40	13.57	0.230	GAL
J015524.9+022818	01 55 24.9	+2 28 16.2	15.10			
J015546.4+071902	01 55 46.4	+7 19 03.8	15.40			
J015935.1+104707	01 59 34.9	+10 46 46.7	15.20			
J075704.9+583245	07 57 06.2	+58 32 58.7	14.50	14.48		
J080132.3+473618	08 01 32.0	+47 36 15.8	15.20		0.158	AGN
J080525.8+753424	08 05 23.7	+75 34 34.7	15.30	14.40		
J080534.6+543132	08 05 34.8	+54 31 30.3	14.90			
J080649.5+751853	08 06 48.3	+75 18 30.7	15.10			
J080938.9+754851	08 09 39.8	+75 48 55.1	14.20		0.094	AGN
J080949.2+521855	08 09 49.2	+52 18 58.2	14.50	14.84	0.138	BL
J081059.0+760245	08 10 58.6	+76 02 42.5	14.20	14.59	0.100	AGN
J081228.3+623627	08 12 28.2	+62 36 23.3	14.50	14.15		

Table 2—Continued

Name (1RXS)	R.A.	Declination	R_{USNO}	V_{GSC}	z	Type
J083045.0+340527	08 30 45.4	+34 05 31.6	15.30		0.063	AGN
J083121.0+483148	08 31 22.3	+48 32 13.9	15.10	15.13		
J083821.6+483800	08 38 22.0	+48 38 01.7	14.80	14.63		
J084255.9+292752	08 42 56.0	+29 27 26.2	15.40		0.193	GAL
J084445.2+765313	08 44 45.3	+76 53 09.3	13.90	15.72	0.131	AGN
J084658.3+704452	08 47 05.7	+70 44 41.1	15.20	14.62		
J085343.5+574846	08 53 44.1	+57 48 41.3	15.00		0.000	STAR
J085358.8+770054	08 53 59.4	+77 00 54.6	15.40			
J085823.0+520533	08 58 24.2	+52 05 40.7	15.10			
J085902.0+484611	08 59 02.9	+48 46 09.0	14.30	14.99	0.083	AGN
J090020.1+503143	09 00 19.1	+50 31 40.5	15.10	14.91		
J090038.4+411409	09 00 38.5	+41 13 55.9	15.10			
J090808.7+500912	09 08 08.8	+50 09 20.0	15.10			
J090950.6+184956	09 09 50.6	+18 49 47.6	15.30			
J091010.2+481317	09 10 10.0	+48 13 41.4	14.30		0.118	AGN
J091254.7+793731	09 12 49.4	+79 37 51.8	14.70	15.59		
J091552.3+090056	09 15 51.8	+9 00 50.9	14.50	12.99	0.000	STAR
J091651.8+523829	09 16 52.0	+52 38 27.9	15.30		0.190	BL
J091904.6+732334	09 19 08.8	+73 23 59.2	15.30			
J091954.9+552120	09 19 55.3	+55 21 36.6	14.90		0.123	AGN
J092246.4+512046	09 22 48.0	+51 20 45.9	14.40	14.80		
J092916.4+501344	09 29 15.7	+50 14 15.7	15.20	13.78		
J093047.9+404446	09 30 47.8	+40 44 41.3	15.30			

Table 2—Continued

Name (1RXS)	R.A.	Declination	R_{USNO}	V_{GSC}	z	Type
J093355.6+141932	09 33 55.9	+14 19 19.9	15.40			
J093427.2+745123	09 34 28.4	+74 51 19.9	14.20			
J093701.0+010548	09 37 01.0	+1 05 43.0	13.60	13.87	0.051	AGN
J093942.8+560247	09 39 43.8	+56 02 30.6	14.10		0.116	AGN
J094617.2+025505	09 46 16.9	+2 54 58.7	15.10			
J094653.0+132000	09 46 52.6	+13 19 53.6	15.20			
J094713.2+762317	09 47 16.7	+76 23 28.2	15.00	14.79		
J095104.2+192531	09 51 03.5	+19 25 32.1	15.30			
J095406.7+212250	09 54 08.1	+21 22 25.5	14.90			
J095652.4+411524	09 56 52.3	+41 15 22.3	15.40	15.00		
J095708.1+243319	09 57 07.2	+24 33 15.6	14.50			
J100050.9+315555	10 00 52.1	+31 56 03.3	15.20			
J100121.5+555351	10 01 20.8	+55 53 52.8	14.80		1.414	AGN
J100335.1+444422	10 03 35.0	+44 44 39.6	15.20			
J100505.4+562426	10 05 06.1	+56 24 29.3	14.80			
J100659.7+673249	10 07 00.8	+67 32 46.8	14.00	14.69		
J100851.6+541451	10 08 54.7	+54 14 45.9	15.40			
J100947.3+523442	10 09 48.5	+52 34 51.2	15.20			
J101238.4+101722	10 12 38.5	+10 17 18.8	14.80			
J101303.2+355131	10 13 03.2	+35 51 23.3	14.60	15.26	0.070	AGN
J101504.3+492604	10 15 04.1	+49 25 59.9	15.20		0.200	BL
J101624.0+333827	10 16 22.9	+33 38 17.0	14.10			
J101645.9+421024	10 16 45.1	+42 10 25.1	13.90		0.054	AGN

Table 2—Continued

Name (1RXS)	R.A.	Declination	R_{USNO}	V_{GSC}	z	Type
J101702.4+390256	10 17 03.6	+39 02 49.4	14.30		0.206	GAL
J101716.7+051145	10 17 16.8	+5 11 49.5	15.00			
J101906.8+231846	10 19 06.7	+23 18 37.0	15.20			
J102236.0+301753	10 22 37.4	+30 17 49.8	14.50	14.71		
J102258.8+202252	10 22 58.2	+20 22 37.5	15.10		0.129	GAL
J102338.5+523356	10 23 39.6	+52 33 49.4	15.20			
J102531.2+514039	10 25 31.2	+51 40 34.7	13.60		0.045	AGN
J102836.6+630255	10 28 37.2	+63 02 48.2	15.00			
J102915.4+572402	10 29 14.8	+57 23 53.1	15.30		0.186	AGN
J102946.7+401914	10 29 46.8	+40 19 13.6	14.70	15.07		
J103134.2+284711	10 31 34.3	+28 47 00.6	15.20		0.060	AGN
J103244.5+391331	10 32 44.2	+39 13 22.6	15.30			
J103422.3+605316	10 34 24.9	+60 53 11.5	15.40			
J103439.8+281755	10 34 39.9	+28 17 41.6	14.80			
J104043.6+330057	10 40 44.0	+33 00 59.5	14.90		0.081	AGN
J104303.0+005423	10 43 02.5	+0 54 17.9	14.80			
J104346.6+223006	10 43 47.0	+22 29 57.4	14.60			
J104427.6+271813	10 44 27.7	+27 18 05.4	14.00			
J104427.6+271813	10 44 27.7	+27 18 05.4	14.00			
J104819.1+521837	10 48 18.0	+52 18 30.3	14.70			
J104926.1+245134	10 49 25.5	+24 51 23.0	14.70			
J105037.1+801204	10 50 35.6	+80 11 50.7	14.90	14.85		
J105124.8+382053	10 51 24.5	+38 20 46.7	15.20			

Table 2—Continued

Name (1RXS)	R.A.	Declination	R_{USNO}	V_{GSC}	z	Type
J105143.8+335936	10 51 43.8	+33 59 26.5	15.10		0.167	AGN
J105151.0+213739	10 51 51.0	+21 37 25.9	14.20			
J105214.2+055514	10 52 15.3	+5 55 08.2	15.00	13.96		
J105355.0+661209	10 53 55.7	+66 12 01.8	15.30			
J105444.4+483145	10 54 44.7	+48 31 38.8	15.40		0.286	AGN
J105519.1+402739	10 55 19.5	+40 27 16.6	15.20		0.120	AGN
J105837.5+562816	10 58 37.7	+56 28 11.4	14.10		0.144	BL
J110237.0+724633	11 02 38.3	+72 46 20.7	15.10			
J110412.4+765859	11 04 13.8	+76 58 58.2	15.40		0.313	AGN
J110537.4+585128	11 05 37.6	+58 51 20.7	15.20			
J110748.8+710538	11 07 52.2	+71 06 01.4	14.40	14.75		
J110831.9+695129	11 08 26.9	+69 51 41.7	15.00			
J111011.4+011333	11 10 12.1	+1 13 27.2	14.50	15.06		
J111422.6+582318	11 14 21.9	+58 23 19.0	14.70		0.206	GAL
J111830.0+402557	11 18 30.4	+40 25 54.5	14.40		0.154	AGN
J111907.1+413018	11 19 07.6	+41 30 03.0	15.40			
J112034.0+100821	11 20 34.2	+10 08 04.5	15.20			
J112147.3+114420	11 21 47.1	+11 44 18.2	13.50	14.48	0.050	AGN
J112349.2+723002	11 23 51.8	+72 30 08.4	15.00	15.09		
J112842.9+633559	11 28 41.6	+63 35 50.5	15.40			
J112850.7+231036	11 28 51.1	+23 10 37.0	15.40			
J112854.0+210630	11 28 55.2	+21 06 30.9	15.30			
J113109.0+263212	11 31 09.3	+26 32 07.8	15.40			

Table 2—Continued

Name (1RXS)	R.A.	Declination	R_{USNO}	V_{GSC}	z	Type
J113302.0+184655	11 33 02.0	+18 47 32.8	15.20			
J113313.3+500837	11 33 12.7	+50 08 56.6	15.00		0.310	GAL
J113630.9+673708	11 36 30.1	+67 37 04.0	15.40		0.135	BL
J113737.4+103931	11 37 38.1	+10 39 30.2	15.30			
J113826.8+032210	11 38 27.1	+3 22 09.9	14.90			
J113849.7+574245	11 38 49.6	+57 42 43.9	13.60		0.115	AGN
J114009.0+030727	11 40 08.7	+3 07 11.0	15.30			
J114106.1+024110	11 41 05.7	+2 41 16.3	15.10			
J114247.5+215717	11 42 45.8	+21 57 22.4	15.30	13.25		
J114509.2+381326	11 45 09.9	+38 13 29.1	15.40			
J114509.3+304724	11 45 10.3	+30 47 16.7	14.30		0.059	AGN
J114606.1+035959	11 46 06.2	+3 59 55.2	14.60			
J114755.3+090235	11 47 55.0	+9 02 28.6	14.50			
J115137.3+561341	11 51 38.1	+56 13 30.8	15.10			
J115553.6+732416	11 55 54.2	+73 23 44.7	15.00	15.65		
J115719.0+333645	11 57 17.4	+33 36 39.9	15.10		0.213	GAL
J115746.9+412642	11 57 46.1	+41 26 37.4	14.40			
J120333.4+022939	12 03 32.9	+2 29 34.5	14.40	13.88	0.077	AGN
J120547.8+584828	12 05 48.9	+58 48 30.0	15.20			
J120954.9+062806	12 09 54.6	+6 28 13.3	14.40			
J121104.0+700536	12 11 03.9	+70 05 31.3	14.00	14.59		
J121157.1+055800	12 11 57.5	+5 58 00.9	14.10			
J121217.1+280356	12 12 16.2	+28 04 07.4	15.40		0.167	AGN

Table 2—Continued

Name (1RXS)	R.A.	Declination	R_{USNO}	V_{GSC}	z	Type
J121417.7+140312	12 14 17.7	+14 03 12.6	13.90	13.96	0.081	AGN
J121510.9+073205	12 15 10.9	+7 32 03.8	15.40		0.136	BL
J121752.1+300705	12 17 52.0	+30 06 59.9	14.40		0.237	BL
J122044.5+690533	12 20 47.9	+69 05 37.7	15.00		*	GAL
J122144.4+751848	12 21 44.0	+75 18 38.5	14.80	14.37	0.070	GAL
J122523.1+042128	12 25 22.9	+4 21 18.6	14.10			
J122623.7+372657	12 26 23.3	+37 27 01.3	15.40			
J122635.9+455933	12 26 36.9	+45 59 40.4	15.10			
J122745.1+084147	12 27 44.8	+8 41 49.8	13.60		0.084	AGN
J122859.5+272527	12 29 00.3	+27 25 21.4	15.10			
J123132.5+641420	12 31 31.3	+64 14 17.5	15.00		0.170	BL
J123154.6+323248	12 31 55.1	+32 32 40.8	14.40			
J123235.8+060315	12 32 35.8	+6 03 09.7	15.10			
J123325.8+093119	12 33 25.8	+9 31 23.0	14.10		0.415	AGN
J123658.8+631111	12 36 58.7	+63 11 12.9	15.20			GAL
J123942.4+342453	12 39 42.5	+34 24 55.7	15.20			
J124129.4+372206	12 41 29.4	+37 22 01.7	13.90		0.063	AGN
J124141.2+344032	12 41 39.9	+34 40 17.6	14.60	14.96		
J124211.3+331703	12 42 10.6	+33 17 02.2	14.10	14.98	0.044	AGN
J124306.2+421233	12 43 07.1	+42 12 31.1	15.30			
J124306.5+353859	12 43 04.2	+35 39 16.8	14.90	15.23		
J124324.2+271645	12 43 24.7	+27 16 48.6	14.70			GAL
J124339.6+700517	12 43 39.3	+70 05 29.9	14.70	15.68		

Table 2—Continued

Name (1RXS)	R.A.	Declination	R_{USNO}	V_{GSC}	z	Type
J124701.3+442325	12 47 00.1	+44 23 13.7	15.30			
J124717.2+481240	12 47 16.3	+48 12 39.6	15.30			
J124818.9+582031	12 48 18.7	+58 20 28.8	14.50			BL
J125005.7+263118	12 50 05.7	+26 31 07.3	15.20		2.043	AGN
J125422.6+793618	12 54 23.1	+79 36 12.8	15.20			
J125801.0+470237	12 57 59.4	+47 02 01.3	14.80			
J125830.1+652121	12 58 27.8	+65 21 30.7	15.40			
J125851.4+235532	12 58 51.4	+23 55 26.6	13.90		0.071	AGN
J130052.9+564101	13 00 50.7	+56 40 51.1	15.40			
J130258.8+162423	13 02 58.8	+16 24 27.7	14.90	15.09	0.067	AGN
J130425.4+333512	13 04 27.2	+33 35 13.0	14.40		0.188	GAL
J130803.0+035124	13 08 03.1	+3 51 14.1	15.10			
J130947.1+081949	13 09 47.0	+8 19 48.9	14.80		0.155	AGN
J131218.0+351524	13 12 17.7	+35 15 20.3	14.70		0.184	AGN
J131334.0+725914	13 13 32.0	+72 59 10.9	15.20		0.112	AGN
J131349.6+365357	13 13 49.0	+36 53 57.7	15.40			
J131414.6+412347	13 14 18.3	+41 24 30.1	15.30			
J131432.5+122706	13 14 32.7	+12 27 17.9	14.70			
J131451.5+421819	13 14 51.5	+42 18 19.1	14.80			
J131555.1+212508	13 15 55.1	+21 25 21.5	15.00			
J131750.4+601047	13 17 50.3	+60 10 40.6	15.30			
J132025.1+690018	13 20 24.6	+69 00 12.4	15.40		0.067	AGN
J132042.4+601526	13 20 45.3	+60 15 16.2	14.00			

Table 2—Continued

Name (1RXS)	R.A.	Declination	R_{USNO}	V_{GSC}	z	Type
J132314.2+463132	13 23 14.9	+46 31 21.8	15.00		0.143	AGN
J132400.2+573918	13 24 00.8	+57 39 16.1	13.90		0.115	BL
J132434.9+475802	13 24 35.5	+47 58 00.7	15.10			
J132602.2+601206	13 26 02.3	+60 11 59.4	15.10			
J132632.2+792850	13 26 32.3	+79 28 51.7	15.00			
J132847.3+503808	13 28 48.5	+50 37 53.5	15.30			
J132908.3+295018	13 29 08.8	+29 50 23.9	15.40		0.047	AGN
J132943.8+315338	13 29 43.6	+31 53 36.3	14.60		0.090	AGN
J133434.3+575019	13 34 35.3	+57 50 15.3	15.00			
J133439.6+171748	13 34 37.3	+17 17 49.4	15.30			
J133608.2+755041	13 36 09.8	+75 50 34.9	15.20	15.28		
J133718.8+242306	13 37 18.7	+24 23 02.9	14.30	14.26	0.107	AGN
J133826.6+321252	13 38 26.9	+32 12 51.9	15.20			
J133908.5+115855	13 39 08.5	+11 58 53.5	15.30			
J133938.5+183055	13 39 37.8	+18 30 59.4	15.10			
J134021.4+274100	13 40 21.9	+27 41 26.8	14.20	14.19		
J134210.9+564219	13 42 10.1	+56 42 10.9	14.60		0.040	AGN
J134335.3+413839	13 43 35.7	+41 38 24.3	14.70	14.60		
J134356.7+253845	13 43 56.7	+25 38 46.9	14.10	15.09		
J134357.3+271252	13 43 57.4	+27 12 40.9	15.40		0.077	AGN
J134453.1+000525	13 44 52.9	+0 05 19.7	14.80	15.51		
J134607.5+293814	13 46 08.1	+29 38 10.5	14.10		0.076	AGN
J135022.2+094007	13 50 22.1	+9 40 10.7	14.00			

Table 2—Continued

Name (1RXS)	R.A.	Declination	R_{USNO}	V_{GSC}	z	Type
J135022.2+094007	13 50 22.1	+9 40 10.7	14.00			
J135143.8+242420	13 51 43.9	+24 24 21.5	14.90			
J135436.0+180523	13 54 35.6	+18 05 17.2	15.30		0.152	AGN
J135553.3+383427	13 55 53.5	+38 34 29.1	15.00		0.051	AGN
J135821.2+360356	13 58 24.5	+36 03 47.7	15.00	15.36		
J140310.5+375810	14 03 08.8	+37 58 27.6	15.20			
J140519.6+020008	14 05 19.4	+2 00 05.2	14.80		0.000	STAR
J140606.1+580045	14 06 04.8	+58 00 41.3	15.30			
J140622.2+222350	14 06 21.9	+22 23 46.7	15.10		0.098	AGN
J140924.1+261827	14 09 23.9	+26 18 21.3	15.40		0.940	AGN
J141336.8+702954	14 13 36.7	+70 29 50.4	14.30		0.107	AGN
J141342.6+433938	14 13 43.7	+43 39 44.1	14.70		0.089	GAL
J141346.6+263246	14 13 45.3	+26 33 03.1	15.00	14.85		
J141700.5+445556	14 17 00.8	+44 56 06.0	14.70	15.17	0.114	AGN
J141756.8+254329	14 17 56.7	+25 43 24.7	15.30		0.237	BL
J141758.8+360749	14 17 58.0	+36 08 10.5	15.20			
J141901.9+280942	14 19 01.9	+28 09 41.7	14.80			
J142058.6+262450	14 20 56.1	+26 24 22.5	15.40	14.95		
J142107.1+253818	14 21 07.6	+25 38 20.8	15.40		1.050	AGN
J142129.8+474719	14 21 29.8	+47 47 24.7	14.30	14.62	0.072	AGN
J142313.4+505537	14 23 14.3	+50 55 38.1	15.20		0.274	AGN
J142425.2+595254	14 24 24.1	+59 53 00.7	15.10	14.18		
J142630.6+390348	14 26 30.7	+39 03 43.5	13.50			

Table 2—Continued

Name (1RXS)	R.A.	Declination	R_{USNO}	V_{GSC}	z	Type
J142700.5+234803	14 27 00.4	+23 48 00.1	14.80			BL
J142725.3+194954	14 27 25.0	+19 49 52.3	14.00	15.60	0.131	AGN
J142906.7+011708	14 29 06.5	+1 17 05.0	13.60	13.21	0.086	AGN
J142924.3+451826	14 29 25.0	+45 18 31.6	15.10			
J143308.8+232650	14 33 08.4	+23 26 31.1	15.10			
J143445.8+332814	14 34 45.3	+33 28 19.8	14.70			
J144034.4+242255	14 40 34.3	+24 22 50.4	15.30			
J144248.5+120042	14 42 48.2	+12 00 40.4	14.60		0.162	BL
J144645.8+403510	14 46 45.9	+40 35 05.8	15.10		0.267	AGN
J144754.0+283323	14 47 54.2	+28 33 23.7	15.40			
J144825.6+355955	14 48 25.0	+35 59 46.4	15.00		0.111	AGN
J145307.6+255438	14 53 08.0	+25 54 32.8	15.40			
J145307.8+215333	14 53 08.3	+21 53 38.5	15.10			
J145559.0+492158	14 55 59.5	+49 21 52.3	15.40			
J145729.4+083356	14 57 29.0	+8 34 22.6	15.00		0.167	AGN
J145843.1+213614	14 58 42.7	+21 36 10.0	15.30		0.062	AGN
J150023.0+763644	15 00 22.3	+76 36 37.7	14.70	15.14		
J150124.1+302638	15 01 24.2	+30 26 33.2	15.30			
J150317.5+681011	15 03 16.3	+68 10 05.7	15.00			
J150332.0+295026	15 03 32.1	+29 50 23.9	14.80			
J150506.8+435002	15 05 07.3	+43 50 05.1	15.00			
J150752.3+515116	15 07 52.6	+51 51 11.1	15.40			
J151040.8+333515	15 10 41.1	+33 35 05.4	15.30			

Table 2—Continued

Name (1RXS)	R.A.	Declination	R_{USNO}	V_{GSC}	z	Type
J151105.3+525128	15 11 06.0	+52 51 26.8	15.00			
J151447.0+351348	15 14 46.9	+35 13 48.6	14.80			
J151634.5+205847	15 16 34.5	+20 58 37.4	14.90			
J151845.3+061340	15 18 45.7	+6 13 55.8	14.40		0.102	AGN
J151921.7+590823	15 19 21.6	+59 08 23.6	14.40	15.09	0.078	AGN
J152558.6+181423	15 25 58.5	+18 14 15.6	15.00			
J152806.5+132337	15 28 06.9	+13 23 50.3	15.20			
J152912.9+381226	15 29 14.0	+38 13 06.0	15.00	15.06	0.000	STAR
J153140.9+201927	15 31 41.3	+20 19 30.1	15.30			
J153202.3+301631	15 32 02.2	+30 16 28.6	13.50	15.30	0.064	BL
J153718.8+084355	15 37 20.5	+8 44 08.7	15.20			
J153935.2+473545	15 39 34.9	+47 35 53.1	15.00	14.87		
J154236.8+581153	15 42 36.9	+58 11 45.0	13.90	14.07		
J154508.1+170935	15 45 07.5	+17 09 50.4	14.70		0.045	AGN
J154732.3+102446	15 47 32.2	+10 24 51.2	15.40			
J154751.7+025538	15 47 51.9	+2 55 50.8	14.70		0.098	AGN
J154814.6+450040	15 48 14.7	+45 00 27.8	14.90			
J155023.8+281125	15 50 24.0	+28 11 17.2	15.20			
J155041.6+413915	15 50 39.0	+41 39 29.9	15.30			
J155411.8+241415	15 54 10.9	+24 14 40.5	15.40			
J155444.6+082202	15 54 44.6	+8 22 21.6	15.40		0.119	AGN
J155543.2+111114	15 55 43.0	+11 11 24.1	14.30	13.81	0.360	BL
J155643.0+294838	15 56 42.8	+29 48 47.5	13.90	14.63	0.087	AGN

Table 2—Continued

Name (1RXS)	R.A.	Declination	R_{USNO}	V_{GSC}	z	Type
J155745.0+353020	15 57 42.3	+35 30 29.9	13.90			
J155818.7+255118	15 58 18.8	+25 51 24.4	15.30		0.070	AGN
J160529.2+720852	16 05 26.0	+72 08 36.3	15.20			
J160740.7+254106	16 07 40.2	+25 41 12.6	13.80	13.87		
J161047.7+330329	16 10 47.8	+33 03 37.7	14.10		0.097	AGN
J161413.0+260412	16 14 13.2	+26 04 15.9	15.10		0.131	AGN
J161601.3+323222	16 16 01.8	+32 32 28.8	15.10		0.118	AGN
J161711.4+063816	16 17 10.5	+6 38 43.0	15.20		0.092	AGN
J161804.5+672409	16 18 03.8	+67 23 50.0	15.00			
J161809.2+361951	16 18 09.4	+36 19 57.8	13.80		0.034	AGN
J161814.2+293828	16 18 14.0	+29 38 08.9	15.30			
J162011.5+172413	16 20 11.3	+17 24 27.5	15.20		0.114	AGN
J162100.4+254547	16 21 00.3	+25 46 03.3	14.70			
J162114.3+181936	16 21 14.4	+18 19 49.9	15.20		0.125	AGN
J162348.2+402948	16 23 48.2	+40 29 59.0	15.00			
J162355.9+370018	16 23 56.4	+37 00 44.9	15.30			
J162456.7+755457	16 24 56.5	+75 54 55.8	13.70		0.200	AGN
J162607.6+335902	16 26 07.2	+33 59 15.0	14.80		0.204	AGN
J163116.3+095545	16 31 16.0	+9 55 57.9	15.00		0.092	AGN
J163323.3+471848	16 33 23.5	+47 19 00.1	14.60		0.116	AGN
J163338.4+371311	16 33 38.7	+37 13 14.8	14.70			
J163509.5+343956	16 35 09.2	+34 40 03.4	15.40			
J163523.2+545304	16 35 23.2	+54 53 00.3	15.00			

Table 2—Continued

Name (1RXS)	R.A.	Declination	R_{USNO}	V_{GSC}	z	Type
J164443.2+261909	16 44 44.1	+26 19 04.6	15.20			
J164550.2+792129	16 45 49.5	+79 21 28.6	14.90			
J164625.8+392922	16 46 26.0	+39 29 32.2	14.60		0.100	AGN
J164735.4+495001	16 47 34.8	+49 49 59.8	14.60		0.047	AGN
J164801.1+295650	16 48 00.8	+29 56 57.4	14.30		0.101	AGN
J165141.2+721824	16 51 39.6	+72 18 42.7	15.40			
J165253.7+400927	16 52 56.6	+40 08 43.1	15.00			
J170328.3+614114	17 03 28.9	+61 41 10.1	14.70			
J170425.2+333145	17 04 22.4	+33 31 40.3	14.90	13.46		
J170535.1+334011	17 05 34.9	+33 40 12.3	14.90			
J171013.2+334410	17 10 13.5	+33 44 03.6	14.80		0.208	AGN
J171322.8+325631	17 13 22.6	+32 56 28.8	14.50		0.100	AGN
J171410.8+575826	17 14 11.5	+57 58 33.5	14.90		0.092	AGN
J171601.3+311215	17 16 01.9	+31 12 13.5	14.40	15.48	0.111	AGN
J171935.9+424518	17 19 33.9	+42 45 22.5	15.00			
J172320.5+341756	17 23 20.8	+34 17 57.8	14.50		0.206	AGN
J172609.3+743103	17 26 08.3	+74 31 03.4	14.60		0.052	AGN
J172855.8+515654	17 28 54.6	+51 56 49.2	14.90	14.21		
J173114.5+323250	17 31 15.2	+32 32 58.4	13.90	14.05		
J174025.8+514942	17 40 25.7	+51 49 42.4	14.50			
J174815.0+582333	17 48 15.3	+58 23 35.5	15.00			
J174839.6+530240	17 48 37.6	+53 02 45.4	15.40			
J214923.8+092921	21 49 23.7	+9 28 47.3	15.30			

Table 2—Continued

Name (1RXS)	R.A.	Declination	R_{USNO}	V_{GSC}	z	Type
J215912.7+095247	21 59 12.3	+9 52 43.4	14.90		0.101	AGN
J222602.8+172245	22 26 02.2	+17 22 47.0	15.40			
J224939.6+110016	22 49 39.6	+11 00 29.2	14.80		0.084	AGN
J225207.7+145448	22 52 08.1	+14 54 49.6	14.80		0.130	AGN
J225636.8+052522	22 56 36.5	+5 25 17.2	14.90		0.066	AGN
J225932.9+245505	22 59 32.9	+24 55 05.6	13.50	15.07	0.034	AGN
J231357.3+144424	23 13 56.3	+14 43 53.5	14.90			
J231517.5+182825	23 15 17.1	+18 28 14.4	15.00		0.104	AGN
J232339.1+090842	23 23 39.0	+9 08 50.6	14.80		0.068	AGN
J233606.6+241555	23 36 06.1	+24 15 58.3	14.50		0.039	AGN
J233641.8+235526	23 36 42.2	+23 55 29.0	14.20		0.127	GAL
J233739.8+001604	23 37 40.7	+0 16 35.3	14.90			
J234031.5+102934	23 40 31.0	+10 29 39.0	14.70			
J234339.0+024445	23 43 39.8	+2 45 03.9	15.40		0.091	AGN
J235257.1+032008	23 52 58.0	+3 20 17.3	14.30		0.086	AGN
J235754.3+132418	23 57 53.8	+13 24 09.6	15.30			

Table 2. THE GSC SAMPLE

Name (1RXS)	R.A.	Declination	V_{GSC}	z	Type
J000350.4+020340	00 03 49.7	+2 03 58.9	13.28		
J001219.0+100602	00 12 19.3	+10 06 45.8	14.02		
J003633.7+254513	00 36 32.4	+25 45 18.2	14.32		
J004400.0+313729	00 44 00.0	+31 37 04.3	14.42		
J004719.4+144215	00 47 19.4	+14 42 11.8	14.00	0.039	AGN
J004931.6+112832	00 49 32.0	+11 28 26.0	14.37	0.275	AGN
J005017.9+083734	00 50 17.4	+8 37 35.3	14.31		
J005029.2+112902	00 50 27.9	+11 29 10.9	14.37	0.000	STAR
J005351.3+221222	00 53 50.9	+22 12 13.7	14.38		
J005953.3+314934	00 59 53.3	+31 49 37.4	13.74	0.015	AGN
J010014.0+055200	01 00 14.1	+5 51 54.8	14.00		
J011125.4+152625	01 11 24.8	+15 26 26.8	13.59		
J011704.2+000025	01 17 03.6	+0 00 27.0	14.50	0.040	AGN
J012732.9+191043	01 27 32.5	+19 10 43.8	11.80	0.017	AGN
J015240.2+014718	01 52 39.6	+1 47 16.8	13.92	0.080	BL
J015242.1+010040	01 52 41.9	+1 00 25.1	13.57	0.230	GAL
J020026.7+024012	02 00 26.3	+2 40 09.9	12.77	0.078	AGN
J024920.8+191813	02 49 20.7	+19 18 14.2	14.18	0.031	AGN
J025153.2+222735	02 51 53.7	+22 27 35.7	12.40	0.000	STAR
J075704.9+583245	07 57 06.2	+58 32 58.7	14.48	0.168	AGN
J080525.8+753424	08 05 23.7	+75 34 34.7	14.40		
J081228.3+623627	08 12 28.2	+62 36 23.3	14.15		
J081517.8+460429	08 15 16.9	+46 04 30.7	14.24		

Table 2—Continued

Name (1RXS)	R.A.	Declination	V_{GSC}	z	Type
J081917.9+642943	08 19 17.6	+64 29 40.0	14.40	0.039	AGN
J082407.3+613612	08 24 11.3	+61 36 11.3	14.01		
J083137.6+192339	08 31 38.3	+19 23 45.2	11.43		
J083811.0+245336	08 38 10.9	+24 53 42.4	12.80		
J084456.2+425826	08 44 56.6	+42 58 35.1	14.40		
J084602.9+830757	08 46 17.9	+83 07 43.5	14.47		
J084742.5+344506	08 47 42.5	+34 45 03.8	13.64	0.064	AGN
J090008.1+743419	09 00 03.7	+74 34 26.4	14.37		
J091230.8+155531	09 12 31.0	+15 55 24.3	13.42		
J091552.3+090056	09 15 51.8	+9 00 50.9	12.99	0.000	STAR
J091826.2+161825	09 18 26.0	+16 18 19.2	13.21	0.030	AGN
J092030.8+013544	09 20 31.1	+1 35 37.1	14.14		
J092108.2+480201	09 21 11.3	+48 01 59.2	13.84		
J092343.0+225437	09 23 43.0	+22 54 32.7	13.43		
J092512.3+521716	09 25 13.0	+52 17 11.4	13.66	0.036	AGN
J092603.6+124406	09 26 03.3	+12 44 03.3	13.71	0.028	AGN
J092702.8+390221	09 27 04.0	+39 02 17.8	13.59		
J092705.7+374157	09 27 03.0	+37 42 05.5	14.12		
J093701.0+010548	09 37 01.0	+1 05 43.0	13.87	0.051	AGN
J093900.4+253008	09 39 00.4	+25 30 14.6	14.41		
J094204.0+234106	09 42 04.8	+23 41 06.5	14.15	0.021	GAL
J094432.8+573544	09 44 04.7	+57 33 28.1	14.13		
J094851.0+153901	09 48 50.2	+15 38 34.6	14.25		

Table 2—Continued

Name (1RXS)	R.A.	Declination	V_{GSC}	z	Type
J095340.4+014154	09 53 41.3	+1 42 01.7	13.98		
J095624.5+064803	09 56 23.8	+6 48 01.6	14.34		
J095919.3+435033	09 59 19.2	+43 50 35.4	13.57		
J100446.0+144651	10 04 47.6	+14 46 45.2	14.23	0.082	AGN
J100641.5+213955	10 06 43.6	+21 39 27.7	14.50		
J101218.6+631133	10 12 21.6	+63 11 32.1	14.21		
J101718.0+291439	10 17 18.3	+29 14 33.8	13.96	0.048	AGN
J101912.1+635802	10 19 12.6	+63 58 02.2	13.69	0.041	AGN
J102334.6+443346	10 23 35.0	+44 33 41.5	13.86		
J102407.0+273130	10 24 06.7	+27 31 22.7	14.22		
J102611.1+523755	10 26 06.2	+52 37 56.3	13.99		
J104038.7+373233	10 40 39.0	+37 32 31.3	13.36		
J104333.4+010109	10 43 32.8	+1 01 08.6	13.99	0.072	AGN
J104439.4+384541	10 44 39.1	+38 45 34.8	14.48	0.036	GAL
J105121.3+360728	10 51 21.3	+36 07 27.4	13.31		
J105214.2+055514	10 52 15.3	+5 55 08.2	13.96		
J105328.5+053052	10 53 29.7	+5 30 30.2	13.92		
J105340.7+525310	10 53 41.2	+52 53 01.7	14.25		
J110159.1+572316	11 02 00.1	+57 22 50.3	14.43		
J110310.2+363911	11 03 10.7	+36 39 06.3	13.41		
J110321.2+133759	11 03 21.8	+13 37 52.4	12.90		
J110455.7+433421	11 04 56.0	+43 34 03.0	14.29		
J110943.6+214519	11 09 41.1	+21 44 24.2	14.33	0.032	GAL

Table 2—Continued

Name (1RXS)	R.A.	Declination	V_{GSC}	z	Type
J111300.1+102518	11 13 00.2	+10 25 12.3	14.29		
J111349.5+093518	11 13 49.7	+9 35 10.9	12.42	0.029	AGN
J112147.3+114420	11 21 47.1	+11 44 18.2	14.48	0.050	AGN
J112150.8+405147	11 21 51.2	+40 51 46.4	13.97		
J112315.6+193610	11 23 14.6	+19 35 25.5	14.13		
J112536.7+542243	11 25 36.1	+54 22 56.9	14.33	0.021	AGN
J114116.2+215624	11 41 16.2	+21 56 21.1	13.25	0.063	AGN
J114516.1+794054	11 45 16.1	+79 40 52.6	13.50	0.065	AGN
J114738.0+050119	11 47 37.4	+5 01 09.3	12.09		
J114741.4+001524	11 47 41.7	+0 15 24.1	14.23		
J115658.6+241523	11 56 55.8	+24 15 35.2	13.55	0.142	GAL
J120333.4+022939	12 03 32.9	+2 29 34.5	13.88	0.077	AGN
J120829.9+132752	12 08 29.8	+13 28 06.0	13.31		
J121417.7+140312	12 14 17.7	+14 03 12.6	13.96	0.081	AGN
J121607.4+504926	12 16 07.0	+50 49 30.2	14.25	0.031	AGN
J121900.7+110727	12 18 59.8	+11 07 53.9	13.53		
J121920.9+063838	12 19 21.5	+6 38 43.9	13.22		
J122005.9+650552	12 20 10.3	+65 05 55.2	14.34		
J122144.4+751848	12 21 44.0	+75 18 38.5	14.37	0.070	AGN
J122147.1+015637	12 21 46.6	+1 56 35.3	13.76		
J122306.6+103722	12 23 06.7	+10 37 16.8	12.25	0.026	GAL
J122324.4+024040	12 23 24.2	+2 40 44.9	12.81	0.023	AGN
J122512.5+321354	12 25 13.1	+32 14 00.9	14.38	0.061	AGN

Table 2—Continued

Name (1RXS)	R.A.	Declination	V_{GSC}	z	Type
J122906.5+020311	12 29 06.7	+2 03 08.1	12.26	0.158	AGN
J123014.2+251805	12 30 14.2	+25 18 05.9	14.49	0.135	BL
J123055.5+315207	12 30 55.8	+31 52 16.1	14.19		
J123203.6+200930	12 32 03.6	+20 09 29.6	12.87	0.064	AGN
J123415.2+481306	12 34 16.0	+48 13 06.9	14.31		
J123651.1+453907	12 36 51.2	+45 39 04.4	13.59	0.290	AGN
J123658.6+455341	12 36 57.0	+45 53 26.0	14.41		
J124147.5+564506	12 41 46.7	+56 45 13.5	13.13		
J124312.5+362743	12 43 12.7	+36 27 43.8	11.42		
J124955.0+102312	12 49 54.5	+10 23 08.3	14.03		
J125731.7+354313	12 57 32.7	+35 43 19.9	14.19		
J130934.9+285908	13 09 36.1	+28 59 15.0	13.95		
J131957.2+523533	13 19 58.8	+52 35 27.7	13.49		
J132016.3+330828	13 20 14.7	+33 08 36.1	13.17	0.036	GAL
J133451.1+374616	13 34 51.9	+37 46 20.7	13.83		
J133718.8+242306	13 37 18.7	+24 23 02.9	14.26	0.107	AGN
J133752.7+204634	13 37 50.9	+20 46 39.8	14.20		
J134021.4+274100	13 40 21.9	+27 41 26.8	14.19		
J134952.7+020446	13 49 52.8	+2 04 44.3	13.32		
J135119.8+033722	13 51 20.2	+3 37 16.4	13.77		
J135304.8+691832	13 53 03.4	+69 18 29.5	12.92		
J135420.2+325547	13 54 20.0	+32 55 47.9	12.78	0.026	AGN
J140226.8+054103	14 02 26.3	+5 40 51.8	13.26		

Table 2—Continued

Name (1RXS)	R.A.	Declination	V_{GSC}	z	Type
J141722.1+452544	14 17 21.9	+45 25 46.7	13.94		
J141759.6+250817	14 17 59.2	+25 08 13.2	11.02		
J141802.6+800710	14 17 59.3	+80 07 02.2	14.19		
J142425.2+595254	14 24 24.1	+59 53 00.7	14.18		
J142906.7+011708	14 29 06.5	+1 17 05.0	13.21	0.086	AGN
J143104.8+281716	14 31 04.8	+28 17 14.8	13.43	0.046	AGN
J143452.3+483938	14 34 52.4	+48 39 42.6	13.38		
J143729.6+412842	14 37 29.9	+41 28 35.2	13.70		
J144713.2+570205	14 47 13.0	+57 01 56.7	13.97		
J150401.5+102620	15 04 01.2	+10 26 16.2	14.19	0.036	AGN
J150406.7+485856	15 04 07.1	+48 58 55.1	14.05		
J150724.6+433356	15 07 23.5	+43 33 51.6	13.64		
J150950.2+415540	15 09 49.7	+41 55 38.8	14.29		
J151750.8+050615	15 17 51.7	+5 06 27.4	13.98	0.039	AGN
J151837.9+404506	15 18 38.9	+40 45 00.0	14.19		
J153345.9+690037	15 33 44.7	+69 00 34.0	13.73		
J153412.6+625902	15 34 13.2	+62 58 57.7	13.76		
J153522.9+600515	15 35 24.5	+60 05 15.3	13.17		
J153552.0+575404	15 35 52.4	+57 54 08.5	13.91	0.030	AGN
J153704.2+374830	15 37 04.0	+37 48 26.9	13.43		
J153944.2+275113	15 39 43.9	+27 50 58.1	13.74		
J154236.8+581153	15 42 36.9	+58 11 45.0	14.07		
J154348.9+401343	15 43 50.5	+40 13 41.6	13.05		

Table 2—Continued

Name (1RXS)	R.A.	Declination	V_{GSC}	z	Type
J154532.3+420500	15 45 34.7	+42 05 07.2	13.87		
J155305.9+445749	15 53 05.1	+44 57 39.9	14.16		
J155532.2+351207	15 55 32.7	+35 11 54.8	13.41		
J155543.2+111114	15 55 43.0	+11 11 24.1	13.81	0.360	BL
J155625.4+090311	15 56 26.0	+9 03 19.2	14.47	0.042	AGN
J155703.2+635029	15 57 03.3	+63 50 27.4	14.01	0.030	AGN
J155721.3+445902	15 57 22.6	+44 58 54.3	14.16		
J155909.5+350144	15 59 09.7	+35 01 47.3	14.14	0.031	AGN
J160740.7+254106	16 07 40.2	+25 41 12.6	13.87		
J161004.4+671030	16 10 04.0	+67 10 25.9	13.67	0.067	BL
J161124.8+585106	16 11 24.6	+58 51 01.3	14.24	0.032	AGN
J161301.5+371656	16 13 01.7	+37 17 15.2	14.37	0.070	AGN
J161801.9+775230	16 17 59.8	+77 52 34.5	13.55		
J161951.7+405834	16 19 51.3	+40 58 47.5	14.31		
J162013.1+400858	16 20 12.7	+40 09 05.7	14.18		
J162409.7+260421	16 24 09.3	+26 04 31.4	14.03	0.040	AGN
J162552.9+434654	16 25 53.3	+43 46 51.9	13.70		
J162903.6+361911	16 29 05.3	+36 18 58.7	14.45	0.000	STAR
J163056.3+361848	16 30 56.1	+36 18 48.5	14.45		
J165057.5+222653	16 50 57.8	+22 26 47.8	14.29		
J165352.6+394538	16 53 52.2	+39 45 36.3	11.27	0.033	BL
J165551.7+214559	16 55 51.4	+21 46 01.2	13.79		
J171227.2+355256	17 12 28.5	+35 53 02.1	13.73	0.027	AGN

Table 2—Continued

Name (1RXS)	R.A.	Declination	V_{GSC}	z	Type
J171959.4+241202	17 19 59.7	+24 12 07.6	14.08		
J172855.8+515654	17 28 54.6	+51 56 49.2	14.21		
J173114.5+323250	17 31 15.2	+32 32 58.4	14.05		
J174700.3+683626	17 46 59.8	+68 36 36.1	13.78	0.063	GAL
J174702.0+493803	17 47 03.0	+49 38 19.3	14.20		
J213740.3+013711	21 37 39.9	+1 37 16.4	13.35		
J222408.1+172903	22 24 08.1	+17 28 47.4	14.42		
J225314.2+040957	22 53 11.9	+4 10 36.1	14.35		
J225453.7+241449	22 54 55.1	+24 14 45.5	14.18		
J230315.7+085226	23 03 15.6	+8 52 26.9	11.05	0.016	AGN
J230706.6+163153	23 07 05.3	+16 32 27.1	13.78		
J231341.0+140113	23 13 40.5	+14 01 15.6	13.86	0.041	AGN
J233413.9+073637	23 34 13.9	+7 37 01.2	13.86		
J234106.5+093805	23 41 06.6	+9 38 09.1	14.38		
J234728.8+242743	23 47 28.8	+24 27 45.8	13.65		
J234953.5+242754	23 49 53.3	+24 27 51.6	13.65		
J235122.7+234417	23 51 21.5	+23 44 24.4	14.02		

Table 3. Other Spectroscopic Identifications

Name (1RXS)	R.A.	Declination	B_J	z	Type
J000011.9+052318	00 00 11.80	+05 23 17.3	16.40	0.039	AGN
J000637.1+434223	00 06 36.60	+43 42 28.3	14.80	0.166	AGN
J000805.6+145027	00 08 05.70	+14 50 23.3	14.50	0.043	AGN
J001409.9+304928	00 14 01.00	+30 49 24.3	18.20	:0.000	STAR
J004649.4+152741	00 46 50.00	+15 27 52.6	16.10	:0.078	AGN
J005050.6+353645	00 50 50.80	+35 36 42.2	14.60	0.056	AGN
J005346.9+223209	00 53 46.20	+22 32 22.5	15.80	0.148	AGN
J011205.2+224452	01 12 05.80	+22 44 38.6	15.80	0.000	STAR
J020012.5+130317	02 00 13.90	+13 03 13.1	16.20	0.000	STAR
J130710.9+394540	13 07 11.50	+39 45 33.1	15.40	0.076	AGN
J144240.3+262330	14 42 40.80	+26 23 32.4	16.40	:0.110	AGN
J151601.5+020055	15 16 01.40	+2 00 59.8	16.80	0.105	AGN
J170320.4+373731	17 03 20.10	+37 37 23.8	16.20	*	AGN
J171235.5+245037	17 12 35.80	+24 50 26.8	17.50	*	AGN
J221832.8+192527	22 18 31.30	+19 25 42.8	14.40	0.000	STAR
J232841.4+224853	23 28 42.90	+22 49 43.7	15.20	0.000	STAR
J234114.9+142820	23 41 15.90	+14 28 43.7	16.80	0.000	STAR
J235959.1+083355	23 59 59.30	+8 33 54.1	15.40	0.083	AGN

Table 4. The USNO Spectroscopic Follow-up ($0 < \delta < 90$)

R_{min}	R_{max}	AR_{min}	AR_{max}	$AREA$
13.50	15.40	00.00	01.00	315.250
13.50	14.55	01.00	06.00	662.000
13.50	15.40	06.00	08.00	32.750
13.50	14.40	08.00	09.00	366.750
13.50	14.40	09.00	10.00	732.750
13.50	13.90	10.00	11.00	688.000
13.50	14.40	11.00	12.00	652.750
13.50	13.90	12.00	13.00	727.566
13.50	14.60	13.00	14.00	758.042
13.50	14.60	14.00	15.00	781.193
13.50	13.70	15.00	16.00	730.482
13.50	14.60	16.00	17.00	780.750
13.50	14.60	17.00	18.00	388.000
13.50	14.90	18.00	22.00	93.500
13.50	14.50	22.00	24.00	454.750

Table 5. The GSC Spectroscopic Follow-up ($0 < \delta < 90$)

V_{min}	V_{max}	AR_{min}	AR_{max}	$AREA$
11.00	14.00	00.00	02.00	646.250
11.00	14.50	02.00	04.00	298.000
11.00	14.50	04.00	06.00	32.750
11.00	13.50	06.00	08.00	32.750
13.20	14.10	08.00	09.00	366.750
11.00	13.75	09.00	10.00	732.750
13.96	14.10	10.00	11.00	688.000
13.45	13.75	11.00	12.00	652.750
11.85	13.00	12.00	13.00	727.566
11.00	13.35	13.00	14.00	758.042
11.00	13.25	14.00	15.00	781.193
13.80	14.05	15.00	16.00	730.482
11.00	13.75	16.00	18.00	1168.750
11.00	14.50	18.00	20.00	000.000
11.00	14.50	20.00	22.00	935.000
11.00	13.50	22.00	24.00	454.750

Table 6. The Differential QSO Counts

<i>B</i> interval	$\langle B \rangle$	N	log surf.den.
			$mag^{-1}deg^{-2}$
12.5-13.5	13.0	3	-3.34
13.5-14.5	14.2	19	-2.69
14.5-15.5	14.8	24	-2.04

Table 7. The QSO Luminosity Function at $0.04 < z < 0.3$

M_B interval	$< M_B >$	N	log LF
			$Mpc^{-3}mag^{-1}$
-21.5 -22.5	-22.04	3	-6.05
-22.5 -23.5	-23.31	9	-6.84
-23.5 -24.5	-24.10	23	-6.89
-24.5 -25.5	-25.10	11	-7.75
-25.5 -28.5	-26.72	2	-9.35

REFERENCES

- Avni, Y., & Bahcall, J. N. 1980, ApJ, 235, 694
- Banse, K., Crane, P., Ounnas, C. & Ponz, D., 1983. In: Proc. of DECUS, Zurich, p. 87
- Bessel, M. S. 1990, A&AS, 83, 357.
- Boyle B.J., 1992, in "Texas/ESO-CERN Symposium on Relativistic Astrophysics, Cosmology and Particle Physics", ed(s) Barrow J.D., Mestel L. and Thomas P., Ann. N.Y. Acad. of Sci., 647, 14
- Burstein, D., Heiles, C. 1982, AJ, 87, 1165
- Cattaneo, A. astro-ph/9907335
- Cavaliere, A., Perri, M., Vittorini, V. 1997, Mem.S.A.It., 68, 27
- Cristiani, S., Vio, R. 1990, A&A, 227, 385
- Cristiani, S., La Franca, F., Andreani, P., Gemmo, A., Goldschmidt, P., Miller, L., Vio, R., Barbieri, C., Bodini, L., Iovino, A., Lazzarin, M., Clowes, R.G., MacGillivray, H., Gouffes, C., Lissandrini, C., Savage, A. 1995, A&AS, 112, 347
- The Digitized Sky Survey <http://arch-http.hq.eso.org/dss/dss>
- Franceschini, A., La Franca, F., Cristiani, S., Martin-Mirones, J.M. 1994, MNRAS, 269, 683
- Gehrels, N. 1986, ApJ, 303, 346
- Goldschmidt, P., Miller, L., La Franca, F., Cristiani, S. 1992, MNRAS, 256, 65p
- Goldschmidt, P., Miller, L. 1998, MNRAS, 293, 107
- Haiman, Z., Menou, K. astro-ph/9810426

- Hartwick, F.D.A., Schade, D. 1990, ARA&A, 28, 437
- Hasinger, G., Burg, R., Giacconi, R., Schmidt, M., Trümper, J., Zamorani, G. 1998, A&A, 329, 482
- Hewett, P.C., Foltz, C.B. 1994, PASP, 106, 113
- Hewett, P.C., Foltz, C.B., Chaffee, F.H. 1993, ApJ, 406, L43
- Kauffmann, G., Haehnelt, M. astro-ph/9906493
- Köhler, T., Groote, D., Reimers, D., Wisotzki, L. 1997, A&A, 325, 502
- La Franca, F., Franceschini, A., Cristiani, S., Vio, R. 1995, A&A, 299, 19
- La Franca, F., Cristiani, S. 1997, AJ, 113, 1517
- Landolt, A.U. 1992, AJ, 104, 340.
- Lasker, B. M., Sturch, C. R. et al. 1988, ApJS, 68, 1.
- Miyaji, T., Hasinger, G., Schmidt, M. astro-ph/9910410
- Monaco, P., Salucci, P., Danese, L. astro-ph/9907095
- Monet, D. A&AS, 188, 5404.
- Oke, J.B. 1990, AJ, 99, 1621.
- Page, M.J., Carrera, F.J. astro-ph/9909434
- Schmidt, M., Green, R. F. 1983, ApJ, 269, 352
- Véron, M.P., Véron, P., 1998, A Catalogue of Quasars and Active Nuclei, 1998, ESO Scientific report No. 18.

Voges, W., 1992 In ESA, Environment Observation and Climate Modelling Through International Space Projects. Space Sciences with Particular Emphasis on High-Energy Astrophysics p 9-19

Voges, W., Aschenbach, B., Boller, T., Brauninger, H., Briel, U., Burkert, W., Dennerl, K., Englhauser, J., Gruber, R., Haberl, F., Hartner, G., Hasinger, G., Pfeffermann, E., Pietsch, W., Predehl, P., Rosso, C., Schmidt, J. H. M. M., Trümper, J., Zimmermann, H.-U. astro-ph/9909315

Yuan, W., Siebert, J., Brinkmann, W. 1998, A&A, 334, 498

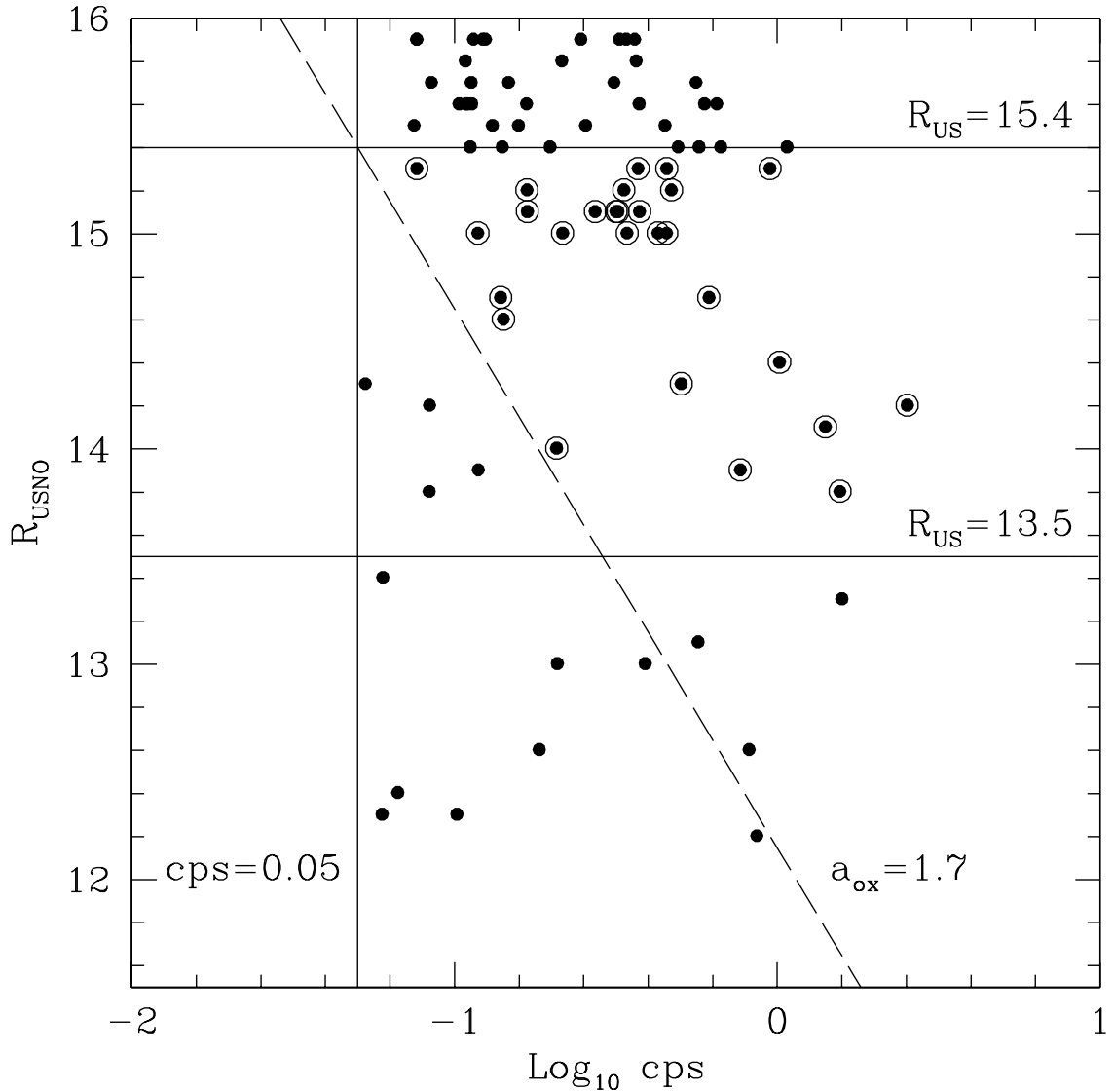


Fig. 1.— The incompleteness in the present selection of quasar candidates is due to objects not found in the RASS catalogue (with a flux ≤ 0.05 cps, on the left of the vertical continuous line) and to the ones with $a_{ox} \geq 1.7$ (on the left of the dashed line).

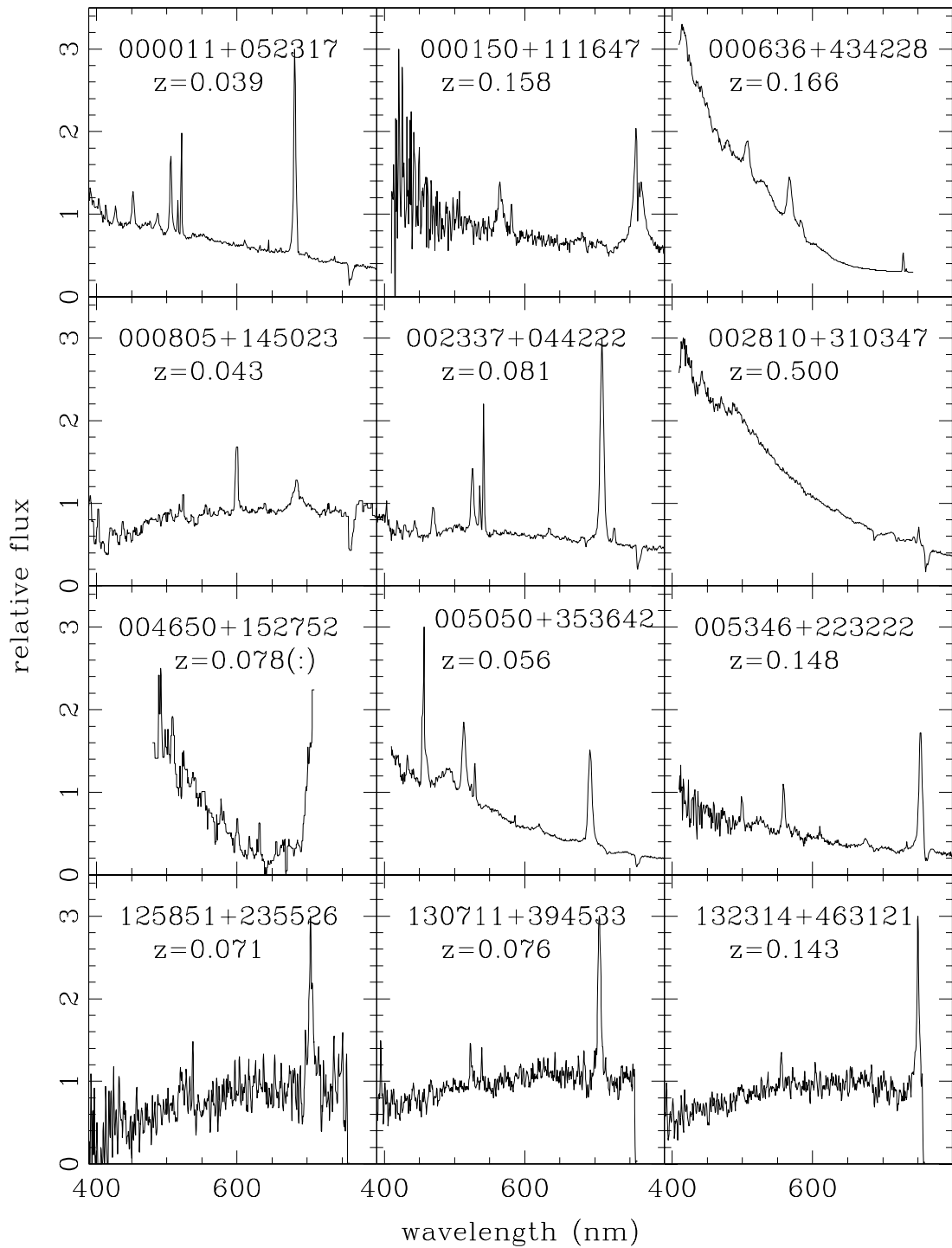


Fig. 2.— a) - The spectra of the AGN confirmed with the follow-up spectroscopy

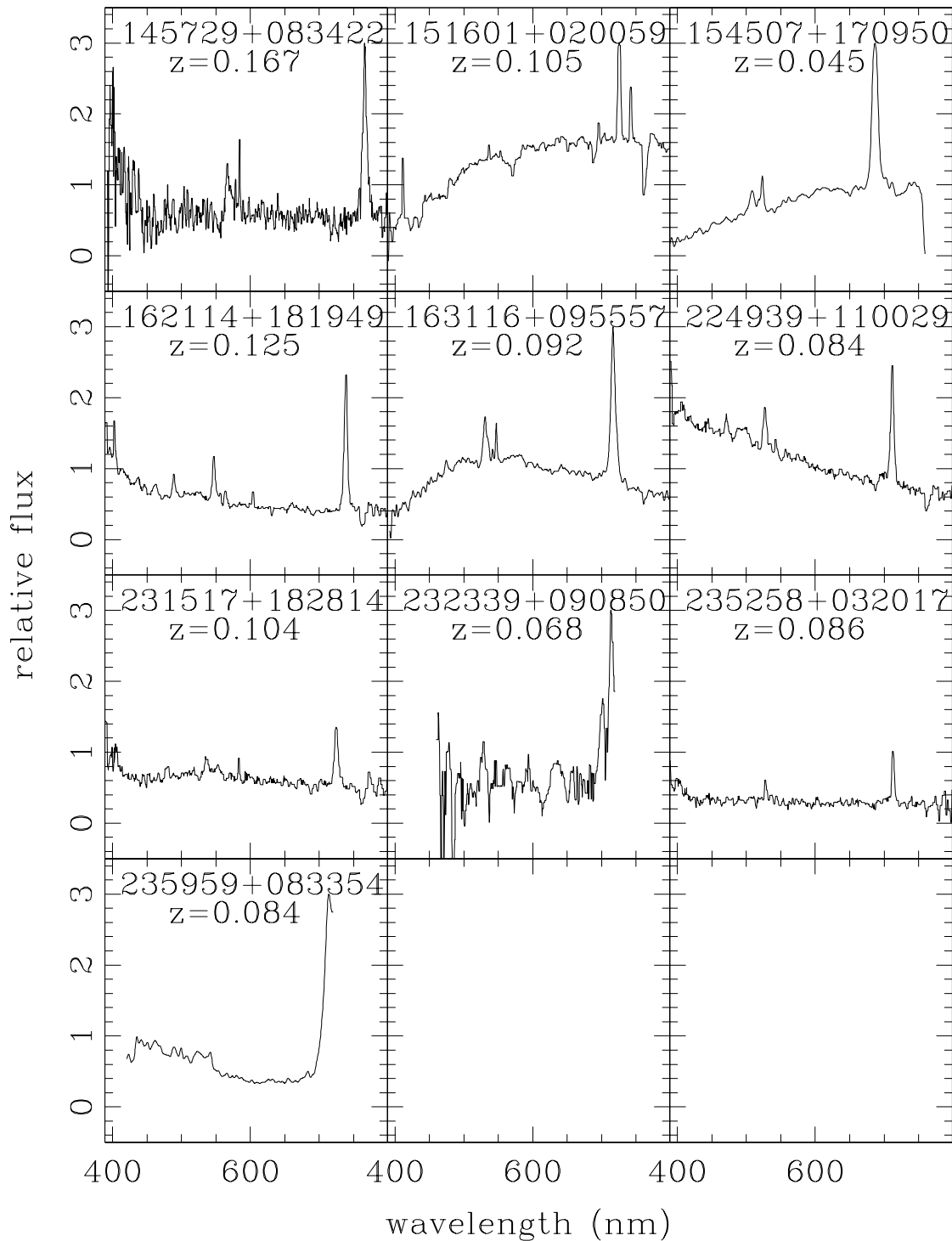


Fig. 2.— b) - The spectra of the AGN confirmed with the follow-up spectroscopy

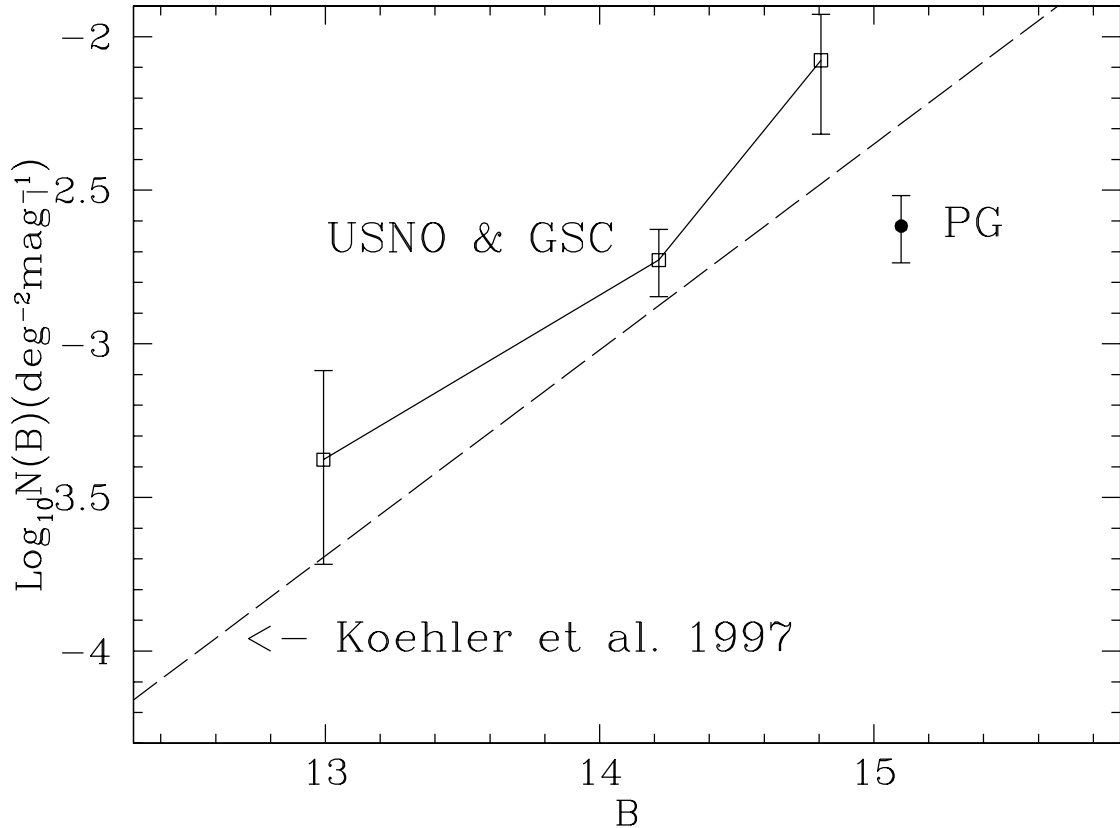


Fig. 3.— The LogN-LogS relation of QSOs. Open squares refer to the present sample and are QSOs with $z \geq 0.04$. A correction of -0.037 to the values of Col. 4 in Tab. 6 has been applied to account for the Bennet bias. The continuous straight line is the relation found by Köhler et al. (1997) for QSOs with $0.07 \leq z \leq 2.2$. The filled circle is the point derived from the PG Survey.

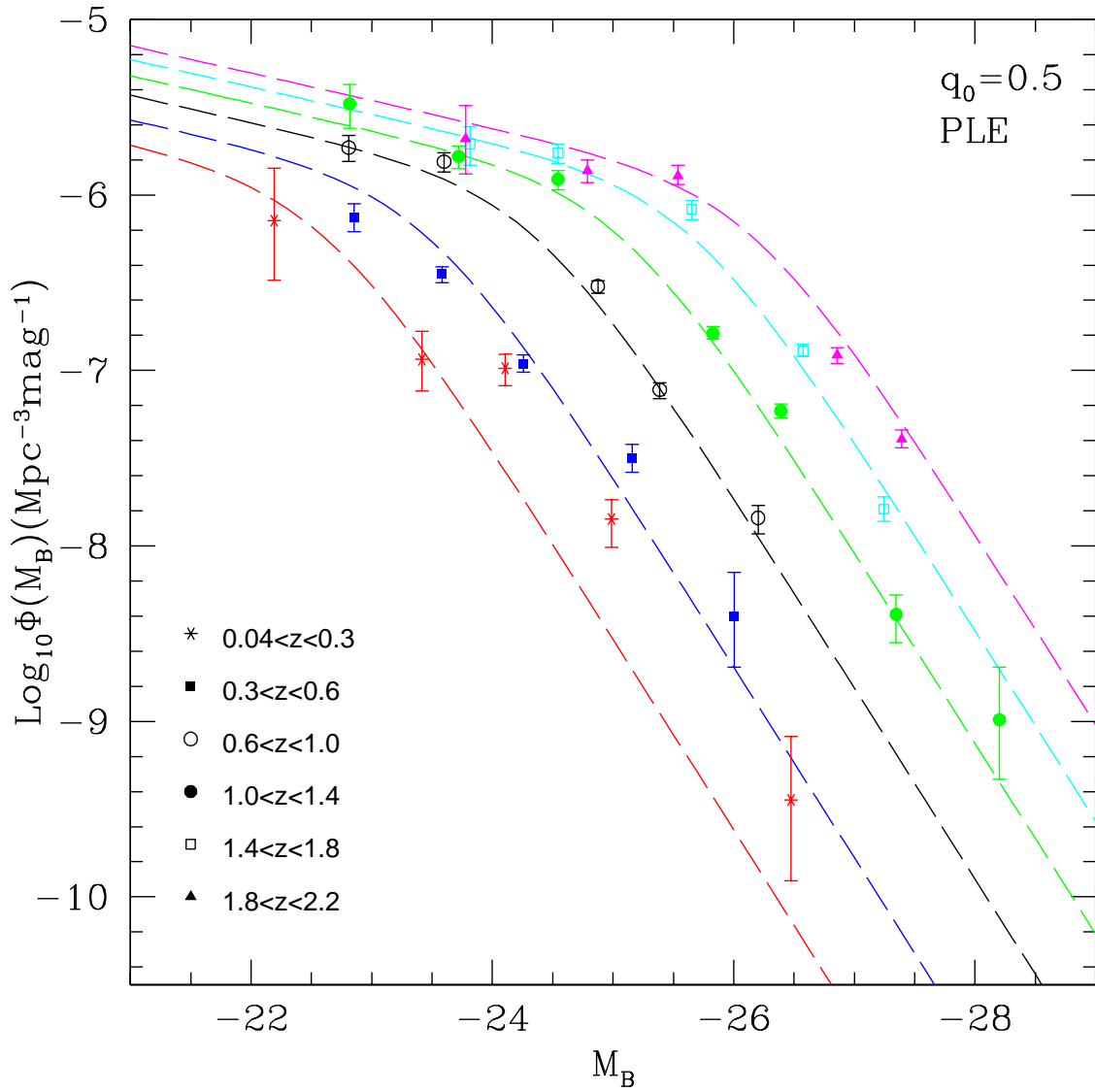


Fig. 4.— a) - The luminosity function of QSOs compared with a parameterization of Pure Luminosity Evolution (see text). The points in the range $0.04 < z \leq 0.3$ are the result of the present survey, the remaining data are derived from LC97.

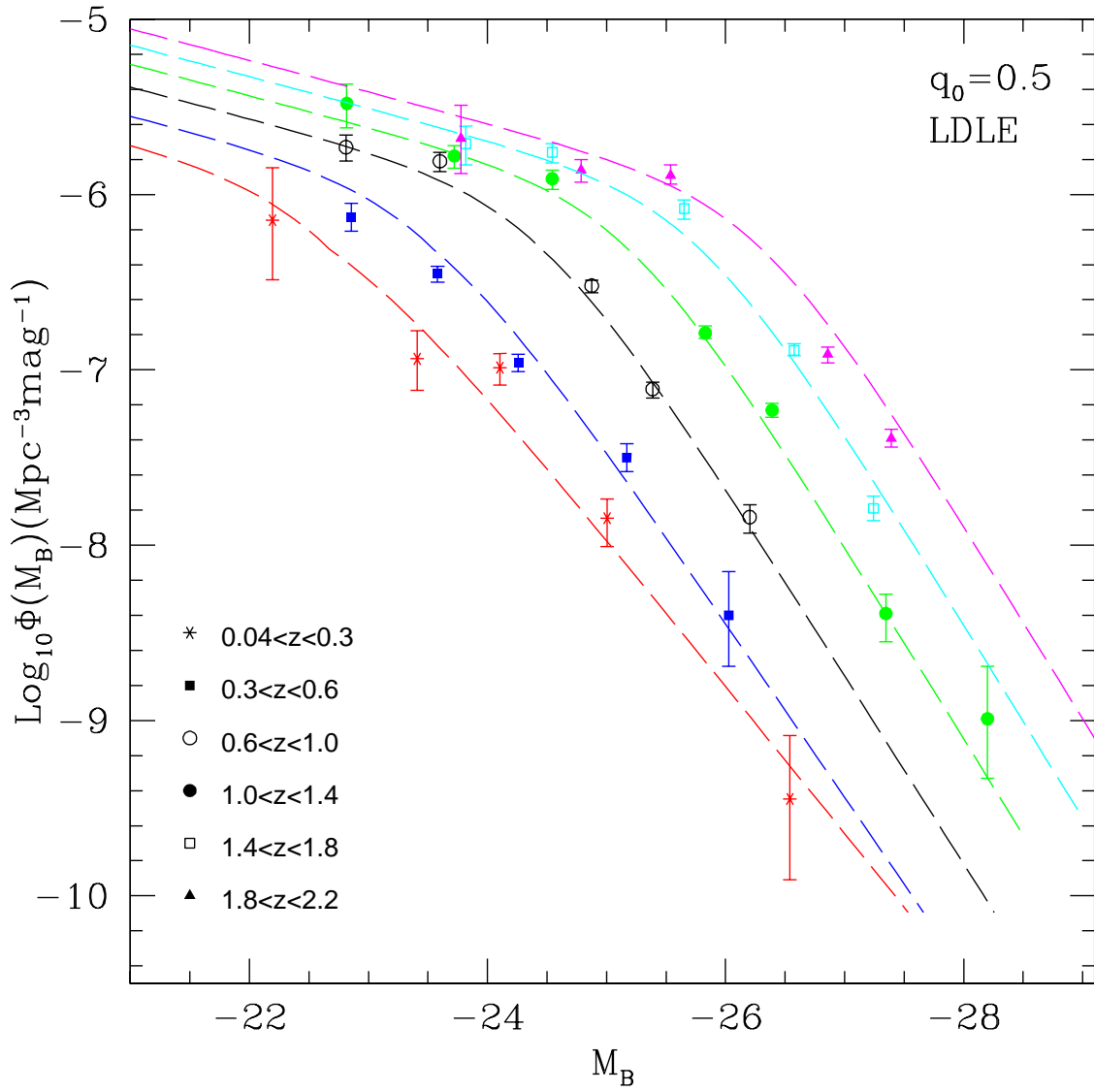


Fig. 4.— b) - The luminosity function of QSOs compared with a parameterization of Luminosity Dependent Luminosity Evolution.

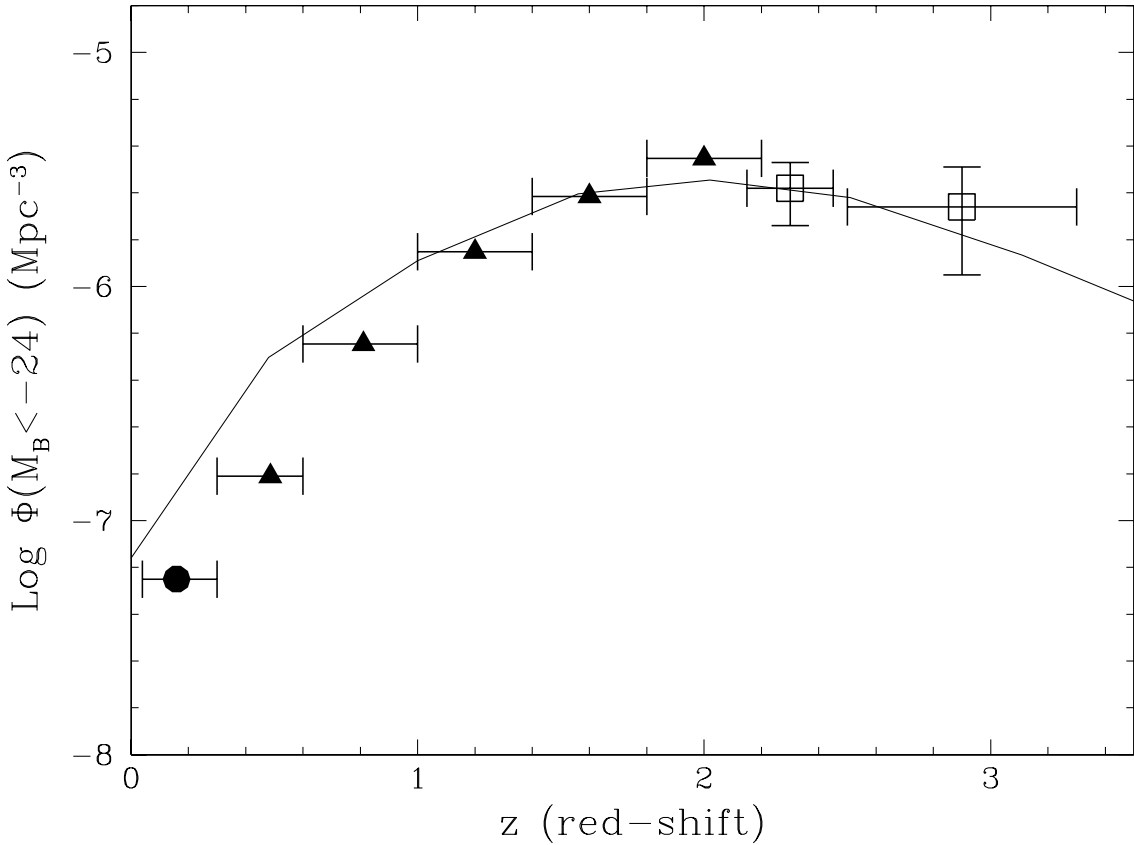


Fig. 5.— The continuous line represents the evolution of the space density of quasars with $M_B < -24$ predicted by the Λ CDM model described in the text (KH99). Filled circles are data from the present work, filled triangles are derived from LC97 and open squares show data from Hartwick & Schade (1990).